S^3Net: A Synthesis-Segmentation-Spiking Network for Alzheimer Disease Detection and Segmentation

***Abstract*—ABSTRACT**

***Index Terms*—Generative Adversarial Network, Deep learning, Alzheimer detection, Alzheimer segmentation, Spike Neural Network**

I. Introduction

II. Related work

Alzheimer's disease (AD) detection has progressed from classic optimization-based segmentation toward advanced deep learning pipelines that analyze imaging data end-to-end. Early work combined bioinspired optimization methods with segmentation to better isolate brain regions such as gray and white matter, improving classification accuracy in later stages [1]. Hybrid loss–driven segmentation models further refined boundary detection, capturing subtle structural changes critical for early diagnosis [2]. These outputs fed into deep architectures like multi-scale CNNs, which learned both fine- and coarse-grained features, boosting robustness against noise and class imbalance [3]. Lightweight multimodal CNN–LSTM frameworks soon emerged, reducing computational demands while maintaining high diagnostic accuracy, making real-time clinical use more practical [4]. Systematic reviews have reinforced that pairing MRI-derived volumetric measures—especially in the medial temporal lobe—with neuropsychological assessments significantly improves early-stage detection over imaging alone [5].

Advances in multimodal fusion brought structural and functional MRI together through spatio-temporal modeling and cross-modal attention, supported by missing-data recovery modules for improved robustness [6]. Biological validation came through transcriptomic studies revealing interneuron alterations linked to known AD biomarkers [7]. Transfer learning and protocol-adaptive designs addressed variability across MRI scanners [8], while dual-decoder adversarial autoencoders paired with residual attention networks improved cross-protocol harmonization [9]. Multimodal feature fusion networks captured structural connectivity and temporal dynamics [10], enabling richer and more comprehensive brain representations that incorporate both micro- and macro-level patterns. Additionally, GAN-based pipelines began synthesizing PET from MRI or augmenting datasets to combat class imbalance, improving model generalization and sensitivity across different disease stages [11]. These GAN approaches not only reduce dependency on costly or less-available imaging modalities but also create diverse, high-quality synthetic samples, thereby enhancing the resilience, adaptability, and performance of deep learning systems in varied clinical and research environments.

Recent developments have advanced these concepts further, incorporating richer clinical and biological information to enhance predictive accuracy. Biomarker-based frameworks have identified hippocampal volume and plasma p-tau as strong predictive markers for AD [12], while clinical research has established links between vascular health, glymphatic clearance, and AD risk [13]. GAN-augmented training pipelines have addressed the limitations of small and imbalanced datasets by generating realistic synthetic samples for underrepresented AD progression stages, improving classification accuracy across multiple disease levels [14], [15], [16]. In parallel, U-Net–based hippocampal localization models have demonstrated high precision in segmenting disease-relevant structures, enhancing both the segmentation stage and downstream classification performance [17], [18]. Hybrid U-Net–GAN frameworks combine high-quality structural segmentation with targeted data augmentation, producing richer and more balanced training sets that improve resilience in deep learning models [15]. The integration of these augmentation strategies has also enabled models to adapt more effectively to unseen patient data, narrowing the gap between experimental accuracy and deployment in hospital settings.

The most recent innovations leverage transformer–hybrid architectures [19] for multimodal fusion and feature enhancement, and reinforcement learning–tuned CNNs optimized with adaptive strategies like CAdam [20], addressing the core challenges of segmentation accuracy, modality integration, dataset harmonization, and robustness for real-world healthcare deployment. Together, these advances demonstrate a clear trajectory from segmentation-focused optimization toward highly integrated, augmentation-driven, and biologically validated deep learning systems. Such frameworks not only aim for high classification accuracy but also prioritize interpretability, enabling clinicians to trust model outputs. By incorporating domain-specific priors, adaptive learning strategies, and scalable cloud-based deployment pipelines, these systems hold the potential to deliver early, reliable, and clinically interpretable AD detection at a population scale, adaptable to both advanced research

hospitals and resource-limited rural healthcare infrastructures

TABLE I: Notation and its description

Notation	Description
O^u, O^v	Original MRI images used for generator (u) and discriminator (v) training batches.
$O_{\text{low}}^{\text{original}}$	Original MRI image dataset used for GAN training.
LoP, LoP_i	Lesion-only patches extracted from MRI images; divided into four subregions ($i = 1$ to 4).
$\mathcal{G}_{gen}$	Synthesized Alzheimer's MRI images generated by the GAN.
f_g	Latent features extracted from the generator's penultimate layer.
f_d	Latent features extracted from the discriminator's intermediate convolutional layer.
I_{orig}	Original or synthesized MRI image used for segmentation.
f_S	Segmentation feature extracted from the final fully connected layer of the segmentation network (input to SNN).
I_i, F_i	Intermediate feature maps from the i-th encoder layer.
D_j, U_j	Feature maps and upsampled activations in the j-th decoder layer.
B	Bottleneck feature representation in the encoder–decoder network.
S_{seg}	Final MRI segmentation map output.
S_n	Spiking neural network input derived from segmentation feature f_S.
f_D	Discriminator features used as input to the SNN (from Algorithm 1).
F_{in}	Integrated feature set combining f_D and f_S for SNN input.
$S_{in}(t)$	Input spike trains encoded from F_{in} over time steps $t = 1, \ldots, T$.
$V_i^l(t)$	Membrane potential of neuron i in layer l at time t.
$S_i^l(t)$	Spike output of neuron i in layer l at time t.
V_{th}	Membrane firing threshold of spiking neurons.
λ	Leak constant controlling membrane decay rate.
T	Total simulation time (number of time steps).
y_{out}	Predicted Alzheimer's class probabilities (AD / CN).
y_{true}	Ground truth class label.
η	Learning rate for parameter updates.
L_{Gen}, L_D	Generator and discriminator loss functions in the GAN.
L_{adv}	Adversarial loss for the generator.
L_{L2}	Pixel-wise mean squared error loss.
L_{SSIM}	Structural similarity loss for MRI quality preservation.
L_{seg}	Combined segmentation loss using Dice and BCE terms.
L_{Dice}	Dice loss component for overlap accuracy.
L_{BCE}	Binary cross-entropy loss for segmentation.
$L_{SpikeCE}$	Spike-based cross-entropy loss for SNN classification.
$\theta_G, \theta_D, \theta_{seg}$	Trainable parameters of the generator, discriminator, and segmentation network.
W_{ij}^l	Synaptic weight between neurons j and i in layer l.
$\sigma(\cdot)$	Sigmoid activation function.
Softmax$(\cdot)$	Softmax activation for output class probabilities.
$BN(\cdot)$	Batch normalization operation.
$Conv_{3\times3}$, $ConvTrans_{3\times3}$	3×3 convolution and transposed convolution operations.
$MaxPool(\cdot)$	Max pooling operation for downsampling.
FC_{final}	Final fully connected layer for feature extraction in the segmentation network.

III. Proposed S^3Net: Synthesis-Segmentation-Spiking Network model

A. Synthesized Network

In the TriNetAD framework, the synthesis stage uses a Generative Adversarial Network (GAN) to create lesion-focused representations that preserve both global and local brain details. The model is trained using the **OASIS-1 dataset**, which includes approximately **80,000 MRI slices** for Alzheimer's Disease analysis, each of size **496 × 248 pixels**. The GAN receives **two inputs** that work together to capture complete structural and pathological information. The first input is the **ground-truth MRI image** from the dataset, which maintains the entire brain structure and spatial consistency. The second input is the **Lesion-Only-Path (SOP)**, representing isolated lesion areas segmented into four divisions. These two inputs are processed simultaneously by the Generator, ensuring that the output not only focuses on lesions but also aligns accurately with the true brain morphology.

The combined input can be represented as

$$I = I_{\text{MRI}} + LOP \tag{1}$$

where I_{MRI} denotes the original ground-truth image and SOP corresponds to the lesion-only path. The Generator combines these two inputs to form a comprehensive representation that contains both global anatomical context and localized lesion information. This merged input enables the network to synthesize lesion-enhanced images that emphasize abnormal regions while maintaining overall brain structure and contrast integrity. Internally, the Generator comprises multiple convolutional layers and skip connections that progressively extract hierarchical feature maps, denoted as f_g, capturing texture variations, boundary details, and spatial dependencies across different scales. These learned representations play a crucial role in ensuring that synthesized lesions are realistic in intensity and shape while remaining structurally aligned with the original MRI context. The feature maps f_g are propagated through successive convolutional blocks, where spatial information is refined at each level, and subsequently fused with feedback signals from the Discriminator during adversarial training. This continuous interaction between the Generator and Discriminator allows the network to iteratively improve the quality of lesion generation, producing synthetic outputs that closely resemble real pathological regions in both appearance and structure.

The Discriminator receives two types of input images: the real ground-truth images from the dataset and the synthetic samples generated by the Generator. It evaluates both inputs to determine authenticity, producing a classification score (real or fake) and generating its own set of feature representations denoted as f_d. These discriminator features are not discarded after evaluation; instead, they are forwarded through concatenation nodes, where f_d is linked with the downstream decoder layers in the segmentation network to refine lesion boundary precision. The Discriminator thus performs a dual role: acting as a critic for adversarial training and as a feature extractor that enhances structural alignment within the overall architecture.

Training the GAN follows a **min-max optimization** where the Generator aims to minimize the objective while the Discriminator tries to maximize it, defined as

$$\min_G \max_D \mathcal{L}_{\text{GAN}}(G, D) \tag{2}$$

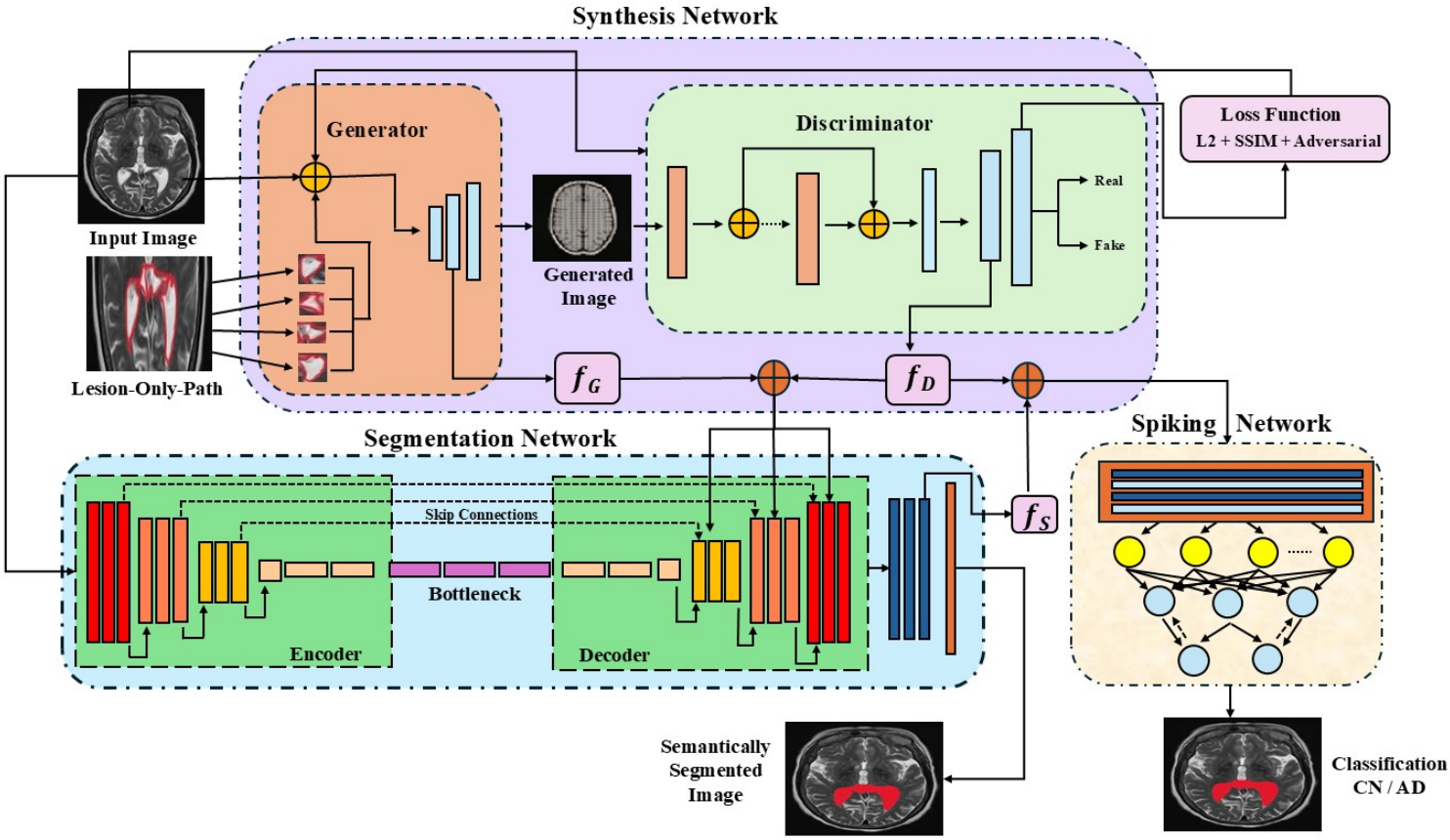

Fig. 1: Illustrates the proposed S^3Net: Synthesis-Segmentation-Spiking Network architecture.

During training, three complementary loss functions collectively guide the optimization of the network, ensuring both structural fidelity and lesion realism. The **adversarial loss** compels the Generator to produce lesion regions that are indistinguishable from real pathological areas by continually competing with the Discriminator, which acts as an adaptive critic. This adversarial interaction helps the model capture subtle intensity variations and complex texture patterns that distinguish normal and abnormal brain tissue. The **L2 regularization loss** enforces pixel-wise similarity between the generated and ground-truth images, reducing blurring artifacts and ensuring spatial accuracy across fine lesion boundaries. In parallel, the **SSIM loss** preserves the overall structural and perceptual consistency of the reconstructed brain slices by emphasizing luminance, contrast, and local correlation between pixels. The combined effect of these three loss components ensures that the synthesized lesions are visually coherent, anatomically consistent with real MRI structures, and maintain a high degree of similarity across all 496 × 248 slices from the OASIS-1 dataset. Gradients derived from these losses are back-propagated through both the Generator and Discriminator, allowing simultaneous refinement of feature extraction, adversarial learning, and the overall quality of lesion synthesis.

Overall, this GAN design ensures that the generated images capture high-fidelity lesion structures, the extracted features f_g and f_d maintain semantic alignment, and the entire synthesis module contributes rich lesion-aware representations for the subsequent stages of the TriNetAD pipeline.

B. Segmentation Network

The U-Net module in the TriNetAD framework is responsible for performing detailed pixel-level lesion segmentation while maintaining both structural precision and contextual awareness across MRI slices. It adopts a symmetric encoder–decoder design that has become a standard choice in medical image segmentation tasks because of its ability to learn from limited data and preserve spatial detail. The encoder functions as a feature extractor, progressively compressing the input representation to capture global context and semantic richness. Each encoder stage consists of consecutive convolutional operations followed by nonlinear activations and pooling layers, which reduce the spatial resolution but expand the depth of the feature maps. This process allows the network to encode texture variations, tissue boundaries, and local intensity patterns that are crucial for distinguishing subtle lesion areas from healthy regions. At the same time, feature normalization ensures that deeper layers maintain stability during training and respond only to meaningful spatial variations in the MRI input.

Algorithm 1 Synthesis of Alzheimer's MRI Images using GAN with Generator, Discriminator, and Feature Extraction for Segmentation

Require: Input MRI images I of size 256×256, learning rate $\eta = 0.0002$, batch size $= 64$, and hyperparameters λ_1, λ_2 for L_2 and L_{SSIM} losses.

Generator:

for each epoch **do**

Sample $\{O^u\}_{u=1}^{n} \sim O_{\text{low}}^{\text{original}}$, a batch of MRI brain images.

Extract lesion-only patches (**LoP**) divided into four defect regions:

$$LoP = \{LoP_1, LoP_2, LoP_3, LoP_4\}$$

Combine original image with corresponding lesion patch:

$$x^u = O^u + L^i, \quad L^i \in LoP$$

Compute generator loss:

$$L_{Gen} = L_{adv} + \lambda_1 L_{L2} + \lambda_2 L_{SSIM} \tag{3}$$

where

$$L_{adv} = -\mathbb{E}[\log D(G(O, LoP))], \tag{4}$$

$$L_{L2} = \frac{1}{N} \sum (O - G(O, LoP))^2, \tag{5}$$

$$L_{SSIM} = 1 - SSIM(O, G(O, LoP)). \tag{6}$$

Extract generator latent features f_g (from the penultimate layer before the FC layer).

Update generator parameters using Adam optimizer:

$$\theta_G \leftarrow \theta_G - \eta \nabla_{\theta_G} L_{Gen}.$$

end for

Synthesized Alzheimer's MRI images $\mathcal{G}_{gen}$ and generator features f_g are passed to the segmentation network.

Discriminator:

for each epoch **do**

Sample real images $\{O^v\}_{v=1}^{m} \sim O_{\text{low}}^{\text{original}}$.

Input to discriminator:

$$x^v = [O^v, \mathcal{G}_{gen}].$$

Compute discriminator loss:

$$L_D = -\mathbb{E}[\log D(O)] - \mathbb{E}[\log(1 - D(G(O, LoP)))] \tag{7}$$

Extract discriminator latent features f_d (from intermediate convolutional layer).

Update discriminator parameters using Adam optimizer:

$$\theta_D \leftarrow \theta_D - \eta \nabla_{\theta_D} L_D.$$

end for

Outputs: Synthesized MRI images $\mathcal{G}_{gen}$, generator features f_g, and discriminator features f_d are forwarded to the segmentation network.

The decoder mirrors the encoder in structure but performs the inverse operation — it gradually restores the spatial resolution through upsampling or transposed convolution while refining the semantic information obtained during encoding. At each level of decoding, feature maps are expanded to their previous spatial size and merged with corresponding encoder features through skip connections. These skip connections are the defining characteristic of the U-Net, enabling the model to reuse shallow-layer information that contains fine details about edges and textures. By directly linking encoder and decoder layers, U-Net effectively compensates for information lost during downsampling and ensures the preservation of boundary precision. This mechanism allows the network to integrate coarse contextual cues from deeper layers with detailed spatial structure from shallower layers, resulting in outputs that are both contextually accurate and visually sharp.

To express the overall segmentation process in simple mathematical form, the U-Net can be represented as

$$S = U(I_{\text{in}}),$$

where I_{in} denotes the input MRI image and S represents the final segmented output highlighting the lesion regions. This relation summarizes the entire forward process — the network $U(\cdot)$ encodes, processes, and reconstructs the MRI slice to produce a pixel-wise lesion probability map. In practice, this means that for every pixel in the input MRI, the U-Net predicts a corresponding value in S that quantifies the likelihood of that pixel belonging to a lesion. The model's design thus ensures a fully differentiable mapping between the input intensity space and the segmentation space, enabling efficient end-to-end optimization.

At the core of the network lies the bottleneck layer, which serves as a compact information bridge between the encoder and decoder. This layer aggregates all encoded features into a condensed latent representation that captures the most critical spatial dependencies and intensity correlations across the MRI slice. By compressing the feature hierarchy into this low-dimensional representation, the network learns how global structures relate to localized patterns, which is essential in detecting small or irregular lesions. During decoding, this compressed information is gradually expanded and refined through successive upsampling blocks, ensuring that every layer reconstructs missing spatial details while maintaining semantic consistency with the original image. The inclusion of skip connections at each decoding level helps to anchor the reconstruction process, guiding the network to reintroduce fine boundary features at the correct spatial positions.

The final stage of the U-Net involves a 1×1 convolution followed by a sigmoid activation function that converts the output feature map into a binary segmentation mask. Each pixel in this output mask represents a probability between 0 and 1, indicating how likely that pixel corresponds to a lesion area. The resulting map is then rescaled to match the original input dimensions of 496×248 pixels, ensuring spatial consistency with the MRI slices from the OASIS-1 dataset. This carefully structured workflow allows the U-Net

to retain global context, recover local structure, and generate highly accurate lesion boundaries even in challenging cases where lesion contrast is low or shapes are irregular. Overall, the U-Net's balance of deep semantic encoding and precise spatial decoding makes it an indispensable component of the TriNetAD framework, delivering robust and anatomically faithful lesion segmentation across all patient scans.

Algorithm 2 Alzheimer's MRI segmentation using integrated generator (f_g) and discriminator (f_d) features within an encoder–decoder network

Require: MRI image I_{orig} (256×256), generator features f_g, discriminator features f_d.

Activation: $\text{LeakyReLU}_{0.2}$ denotes Leaky ReLU with slope 0.2.

Encoder:

for each layer E_i, $i = 1, \ldots, N_e$ **do**

$F_i = \text{LeakyReLU}_{0.2}(BN(Conv_{3\times3}(I_{i-1})))$

$I_i = MaxPool(F_i)$; store F_i for skip connections.

end for

Encoder output: $I_{enc} = I_{N_e}$.

Bottleneck: $B = \text{LeakyReLU}_{0.2}(BN(Conv_{3\times3}(I_{enc})))$

Decoder:

for each layer D_j, $j = N_d, \ldots, 1$ **do**

$U_j = \text{LeakyReLU}_{0.2}(BN(ConvTrans_{3\times3}(B)))$

$F_{dec} = [U_j, F_j, f_g, f_d]$

$D_j = \text{LeakyReLU}_{0.2}(BN(Conv_{3\times3}(F_{dec})))$

end for

Segmentation map:

$$S_{seg} = \sigma(Conv_{1\times1}(D_1)) \tag{8}$$

Segmentation loss:

$$L_{seg} = \alpha L_{Dice} + (1-\alpha) L_{BCE} \tag{9}$$

$$L_{Dice} = 1 - \frac{2|P \cap G|}{|P| + |G|} \tag{10}$$

$$L_{BCE} = -\frac{1}{N} \sum [G \log P + (1-G) \log(1-P)] \tag{11}$$

Parameter update:

$$\theta_{seg} \leftarrow \theta_{seg} - \eta \nabla_{\theta_{seg}} L_{seg}$$

Extract fully connected feature:

$$F_s = FC_{final}(D_1) \tag{12}$$

Feed to Spiking Network(S_n)**:**

$$S_n \leftarrow F_s$$

Output: Segmentation map S_{seg} and Spiking Network input feature F_s.

C. Spiking Network

The final stage of the TriNetAD framework utilizes a Spiking Neural Network (SNN) for subject-level classification into Alzheimer's Disease (AD) or Cognitively Normal (CN) categories. Unlike conventional artificial neural networks, the SNN operates on discrete spike trains, closely mimicking biological neural activity and enabling energy-efficient computation. The input to the SNN is formed by concatenating the segmentation output from U-Net (fu) with the lesion-aware features (Fd) generated by the GAN, providing a combined representation of both structural and pathological information. These inputs are encoded into temporal spike sequences and propagated through layers of spiking neurons modeled using the Leaky Integrate-and-Fire (LIF) dynamics. The firing patterns across neurons capture discriminative temporal dependencies associated with disease progression. The output layer computes spike-based activations, and the class with the highest firing rate is assigned as the predicted label (AD or CN). The SNN is trained using a spike-based cross-entropy loss, ensuring reliable classification performance while maintaining computational efficiency.

D. Overall loss function

The training of the TriNetAD framework uses a **combined loss function** to guide the GAN and U-Net modules effectively. It consists of three main parts:

1. Adversarial Loss (L_{adv}) – This loss helps the GAN generate realistic lesions. The generator tries to fool the discriminator into thinking generated lesions are real, while the discriminator tries to distinguish real from fake. It is defined as:

$$L_{\text{adv}} = \mathbb{E}[\log D(x)] + \mathbb{E}[\log(1 - D(G(z)))] \tag{19}$$

where D is the discriminator, G is the generator, x is a real MRI sample, and z is the input lesion or latent vector.

2. L2 Regularization(L2) This term prevents overfitting by keeping model weights small. It is defined as:

$$L_{\text{L2}} = \lambda \sum_i w_i 2 \tag{20}$$

where w_i are the model weights and λ controls the regularization strength.

3. Structural Similarity Index Loss ($\mathbf{L}_{SSIM}$) – This loss ensures that generated lesions maintain anatomical consistency with the real MRI scans. It is defined as:

$$L_{\text{SSIM}} = 1 - \text{SSIM}(x, G(z)) \tag{21}$$

where $\text{SSIM}(x, G(z))$ measures the similarity between the real image x and the generated image $G(z)$.

4. Overall Loss (L_{total}) – The total loss combines adversarial loss, L2 regularization, and SSIM loss to ensure realistic and structurally faithful generated lesions. It is defined as:

$$L_{\text{total}} = L_{\text{adv}} + \lambda L_{\text{L2}} + \gamma L_{\text{SSIM}} \tag{22}$$

where L_{adv} is the adversarial loss, L_{L2} is the L2 regularization loss, L_{SSIM} is the Structural Similarity Index loss, λ controls the strength of regularization, and γ controls the contribution of SSIM loss.

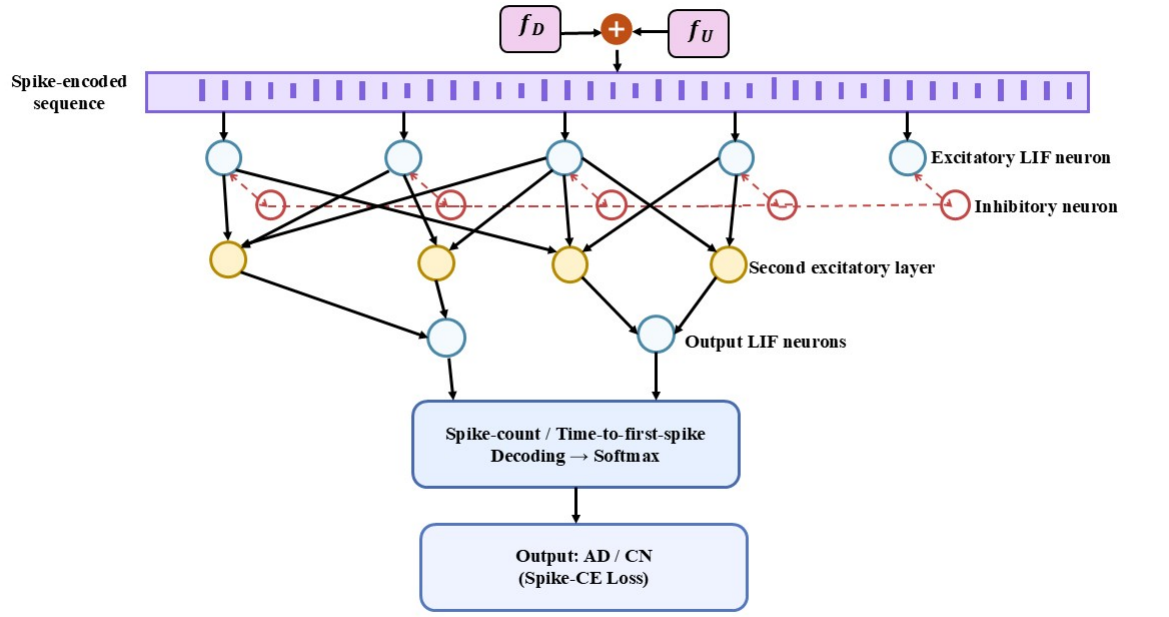

Fig. 2: Illustrates the proposed Spiking Network architecture.

IV. Experiments

A. Dataset

1) OASIS MRI: The OASIS MRI dataset, sourced from the OASIS-1 collection for Alzheimer's Disease research, contains 80,000 MRI images with original slice dimensions of 496 $\times$ 248 pixels [21]. It is categorized into four classes: Non-Demented, Very Mild Demented, Mild Demented, and Demented. The original .nii scans were converted to 2D .jpg slices along the z-axis, with slices 100 to 160 being selected for analysis.

2) Alzheimer's MRI Dataset: The Alzheimer's MRI Dataset is available on Kaggle for Alzheimer's Disease research. It contains 11,519 MRI images. Each image has a pixel size of 128 $times$128 [22]. The dataset is divided into training and testing folders. It includes two classes: Alzheimer's Disease and Cognitively Normal.

3) MRI Dataset: The MRI Dataset (Augmented) is sourced from Kaggle for Alzheimer's Disease research. It consists of 40,000 MRI slices. The original voxel dimensions are 176 $times$208 [23]. The dataset is divided into four classes: Non-Demented, Very Mild Demented, Mild Demented, and Demented. It includes both original scans and augmented images. The augmentation helps improve class balance and diversity.

V. Results

References

[1] Chitradevi Dakshinamoorthy, Prabha S, Sandeep Kumar Mathivanan, Manu Singh, Saurav Mallik, *A comprehensive hybrid model: Combining bioinspired optimization and deep learning for Alzheimer's disease identification*, Computers in Biology and Medicine, Volume 195, 2025, 110654.

[2] Indhumathi G, Palanivelan M, *Alzheimer's disease classification using hybrid loss Psi-Net segmentation and a new hybrid network model*, Computational Biology and Chemistry, Volume 116, 2025, 108375.

[3] Shashank Venkat, Tanmay Ghodeswar, Parth Chavan, Senthil Kumar Narayanasamy, Kathiravan Srinivasan, *MRI-based automated diagnosis of Alzheimer's disease using Alzh-Net deep learning model*, Biomedical Signal Processing and Control, Volume 102, 2025, 107367.

[4] Ejaz Ul Haq, Qin Yong, Zhou Yuan, Xu Huarong, Rizwan Ul Haq, *Multimodal fusion diagnosis of the Alzheimer's disease via lightweight CNN-LSTM model using magnetic resonance imaging (MRI)*, Biomedical Signal Processing and Control, Volume 104, 2025, 107545.

[5] Sabrina Bonarota, Giulia Caruso, Carlotta Di Domenico, Sofia Sperati, Federico Maria Tamigi, Giovanni Giulietti, Federico Giove, Carlo Caltagirone, Laura Serra, *Integration of automatic MRI segmentation techniques with neuropsychological assessments for early diagnosis and prognosis of Alzheimer's disease: A systematic review*, NeuroImage, Volume 314, 2025, 121264.

[6] Wenjun Zhou, Weicheng Luo, Liang Gong, Bo Peng, *Enhanced early diagnosis of Alzheimer's disease with HybridCA-Net: A multimodal fusion approach*, Expert Systems with Applications, Volume 292, 2025, 128580.

[7] Kevin S. Chen, Mohamed H. Noureldein, Diana M. Rigan, John M. Hayes, Kyle J. Loi, Junguk Hur, Masha G. Savelieff, Eva L. Feldman, *Interneuron transcriptomics reveals pathologic markers of Alzheimer's disease progression*, Neurobiology of Disease, Volume 213, 2025, 107012.

[8] Rosanna Turrisi, Sarthak Pati, Giovanni Pioggia, Gennaro Tartarisco, *Adapting to evolving MRI data: A transfer learning approach for Alzheimer's disease prediction*, NeuroImage, Volume 307, 2025, 121016.

[9] Shiyao Li, Shukuan Lin, Yue Tu, Jianzhong Qiao, Shenao Xiao, *Unified multi-protocol MRI for Alzheimer's disease diagnosis: Dual-decoder adversarial autoencoder and ensemble residual shrinkage attention network*, Biomedical Signal Processing and Control, Volume 105, 2025, 107660.

[10] Yibo Huang, Jie Liu, Zhiyong Li, Qiuyu Zhang, *MFIFN: A multimodal feature interaction fusion network-based model for Alzheimer's disease classification*, Biomedical Signal Processing and Control, Volume 107, 2025, 107857.

Algorithm 3 Spiking Network for Alzheimer's Classification

Require: Discriminator features f_D, segmentation features f_S, membrane threshold V_{th}, leak constant λ, simulation time T, and learning rate η.

Feature Integration and Encoding:

Combine features:

$$F_{in} = f_D + f_S \tag{13}$$

Encode F_{in} into spike trains:

$$S_{in}(t) = \text{Encode}(F_{in}), \quad t = 1, 2, \ldots, T \tag{14}$$

Spiking Neuron Dynamics:

for each time step $t = 1$ to T **do**
  for each neuron i in layer l **do**
    Update membrane potential:

$$V_i^l(t) = \lambda V_i^l(t-1) + \sum_j W_{ij}^l S_j^{l-1}(t) \tag{15}$$

    Fire spike if $V_i^l(t) \geq V_{th}$:

$$S_i^l(t) = \begin{cases} 1, & \text{if } V_i^l(t) \geq V_{th} \\ 0, & \text{otherwise} \end{cases} \tag{16}$$

    Reset potential: $V_i^l(t) \leftarrow V_i^l(t) - V_{th} \cdot S_i^l(t)$
  end for
end for

Spike Decoding:

Compute class probabilities:

$$y_{out} = \text{Softmax}\Big(\sum_{t=1}^{T} S^L(t)\Big) \tag{17}$$

Loss and Learning:

Spike cross-entropy loss:

$$L_{SpikeCE} = -\sum_c y_{true}^{(c)} \log(y_{out}^{(c)}) \tag{18}$$

Update weights: $W \leftarrow W - \eta \frac{\partial L_{SpikeCE}}{\partial W}$

Output: Alzheimer's classification label (AD / CN).

[11] Apoorva Sikka, Skand Peri, Jitender Singh Virk, Usma Niyaz, Deepti R. Bathula, *MRI-to-PET cross-modality translation using globally & locally aware GAN (GLA-GAN) for multi-modal diagnosis of Alzheimer's disease*, The Journal of Precision Medicine: Health and Disease, Volume 2, 2025, 100004.

[12] Shehu Mohammed, Neha Malhotra, *Predicting Alzheimer's Disease onset: A machine learning framework for early diagnosis using biomarker data*, Computer Methods and Programs in Biomedicine Update, Volume 8, 2025, 100209.

[13] Ming-Liang Wang, Meng-Meng Yu, Zheng Sun, Jun-Jie Zhang, Jing-Kun Zhang, Xue Wu, Xiao-Er Wei, Yue-Hua Li, *Associations of ischemic heart disease with brain glymphatic MRI indices and risk of Alzheimer's disease*, The Journal of Prevention of Alzheimer's Disease, Volume 12, Issue 3, 2025, 100045.

[14] M. I. Khan, S. Nazir, M. S. Farooq, M. A. Iftikhar, *Generative adversarial networks-based data augmentation for improved Alzheimer's disease classification*, Frontiers in Medicine, Volume 11, 2024, 1443151.

[15] H. Sharma, P. Gupta, *Hybrid U-Net–GAN model for medical image segmentation and augmentation in Alzheimer's detection*, Proceedings of the International Conference on Bioinformatics and Computational Biology, 2024, pp. 54–60.

[16] Y. Li, X. Zhang, L. Wang, *Deep convolutional GAN for synthetic MRI generation in Alzheimer's disease diagnosis*, Journal of Medical Imaging and Health Informatics, Volume 14, Issue 8, 2024, pp. 2345–2354.

[17] K. A. Mehmood, R. Malik, *U-Net–based hippocampal localization for Alzheimer's disease diagnosis*, Bioinformatics and Computational Biology Conference Proceedings, 2024, pp. 21–28.

[18] S. Ahmed, N. Khalid, *High-precision hippocampal segmentation using 3D U-Net for Alzheimer's detection*, Journal of Computational Neuroscience, Volume 39, 2024, pp. 455–468.

[19] Rahma Kadri, Bassem Bouaziz, Mohamed Tmar, Faiez Gargouri, *Innovative multi-modal approaches to Alzheimer's disease detection: Transformer hybrid model and adaptive MLP-Mixer*, Pattern Recognition Letters, Volume 190, 2025, Pages 15–21.

[20] Puja A. Chaudhari, Suhas S. Khot, *Alzheimer's disease prediction using CAdam optimized reinforcement learning-based deep convolutional neural network model*, Biomedical Signal Processing and Control, Volume 108, 2025, 107968.

[21] Daniel S. Marcus, Tracy H. Wang, Jamie Parker, John G. Csernansky, John C. Morris, Randy L. Buckner, *Open Access Series of Imaging Studies (OASIS): Cross-sectional MRI Data in Young, Middle Aged, Nondemented, and Demented Older Adults*, Journal of Cognitive Neuroscience, Volume 19, Issue 9, 2007, 1498–1507. doi: https://doi.org/10.1162/jocn.2007.19.9.

[22] Arif Miad, *Detecting Alzheimer's with Precision 99% Accuracy on OASIS MRI Dataset*, https://github.com/Arif-miad/Detecting-Alzheimer-s-with-Precision-99-Accuracy-on-OASIS-MRI-Dataset-, Accessed: 2025-10-15.

[23] Tourist55, *Alzheimer's Dataset - 4 Class of Images*, Kaggle, https://www.kaggle.com/tourist55/alzheimers-dataset-4-class-of-images, Accessed: 2025-10-15.